This is an almost final version of the paper 'J. Gasteiger, C. Emde, B. Mayer, R. Buras, S.A. Buehler, and O. Lemke. Representative wavelengths absorption parameterization applied to satellite channels and spectral bands. J. Quant. Spectrosc. Radiat. Transfer, 148, 99-115, 2014'.

All changes during the review process are considered, but minor changes performed after acceptance of the paper may be missing.

The final paper is provided at https://doi.org/10.1016/j.jqsrt.2014.06.024 or upon request to developers@libradtran.org

Representative wavelengths absorption parameterization applied to satellite channels and spectral bands

J. Gasteiger[a,*], C. Emde[a], B. Mayer[a], R. Buras[a], S. A. Buehler[b,c], O. Lemke[b,c]

[a] *Meteorologisches Institut, Ludwig-Maximilians-Universität, Theresienstr. 37, München, Germany*
[b] *SRT, Luleå University of Technology, Rymdcampus 1, Kiruna, Sweden*
[c] *Now at: Meteorological Institute, University of Hamburg, Bundesstraße 55, Hamburg, Germany*

Abstract

Accurate modeling of wavelength-integrated radiative quantities, e.g. integrated over a spectral band or an instrument channel response function, requires computations for a large number of wavelengths if the radiation is affected by gas absorption which typically comprises a complex line structure. In order to increase computational speed of modeling radiation in the Earth's atmosphere, we parameterized wavelength-integrals as weighted means over representative wavelengths. We parameterized spectral bands of different widths (1 cm^{-1}, 5 cm^{-1}, and 15 cm^{-1}) in the solar and thermal spectral range, as well as a number of instrument channels on the ADEOS, ALOS, EarthCARE, Envisat, ERS, Landsat, MSG, PARASOL, Proba, Sentinel, Seosat, and SPOT satellites. A root mean square relative deviation lower than 1% from a "training data set" was selected as the accuracy threshold for the parameterization of each band and channel. The training data set included high spectral resolution calculations of radiances at the top of atmosphere for a set of highly variable atmospheric states including clouds and aerosols. The gas absorption was calculated from the HITRAN 2004 spectroscopic data set and state-of-the-art continuum models using the ARTS radiative transfer model. Three representative wavelengths were required on average to fulfill the accuracy threshold. We implemented the parameterized spectral bands and satellite channels in the uvspec radiative transfer model which is part of the libRadtran software package. The parameterization data files, including the representative wavelengths and weights as well as lookup tables of absorption cross sections of various gases, are provided at the libRadtran webpage.

In the paper we describe the parameterization approach and its application. We validate the approach by comparing modeling results of parameterized bands and channels with results from high spectral resolution calculations for atmospheric states that were not part of the training data set. Irradiances are not only compared at the top of atmosphere but also at the surface for which this parameterization approach was not optimized. It is found that the parameterized bands and channels provide a good compromise between computation time requirements and uncertainty for typical radiative transfer problems. In particular for satellite radiometer simulations the computation time requirement and the parameterization uncertainty is low. Band-integrated irradiances at any level as well as heating and cooling rates below 20 km can also be modeled with low uncertainty.

Keywords:
Band parameterization, Satellite channel parameterization, Gas absorption, Radiative transfer, Earth's atmosphere

*Corresponding author. Phone: +49 89 2180 4386, Fax: +49 89 2180 4182, Email: josef.gasteiger@lmu.de.

1. Introduction

Modeling of wavelength-integrated radiative quantities is required frequently in atmospheric science, e.g. for simulating irradiances or radiances measured by remote sensing instruments. It requires the radiative transfer problem to be solved at a large number of wavelengths if the spectral range is affected by fine-structured absorption features of gases, making it computationally expensive. Fine-structured gas absorption features exist in large parts of the visible and infrared spectral range.

Different parameterization approaches are available for reducing the computational cost of such modeling problems. The most prominent general approach is the k-distribution approach. The basic idea of the k-distribution approach is to sort the wavelength grid such that the gas absorption coefficient on the reordered wavelength grid is smooth and monotonic; with the reordered grid, the spectral integration of radiative quantities requires much less wavelength grid points. The optimum ordering depends on pressure, temperature, and gas concentration. Many k-distribution methods use the assumption that the gas absorption spectra of the different atmospheric layers are correlated with the gas absorption spectrum of a reference layer [1]. Such correlated-k distribution methods are used for example by Kato [2] and Fu [3] for wide spectral bands, and by Kratz [4] for AVHRR satellite channels. A k-distribution method not employing the correlation assumption is described for example by Doppler et al. [5] which builds upon the so-called Spectral Mapping Transformation using k-distributions whose validity was tested at all atmospheric layers. Another parameterization approach employing k-distribution methods is LOWTRAN where the transmittance of the gases within 20 cm^{-1} wide bands is approximated by the sum of up to three exponential terms [6]. LOWTRAN7 is implemented in the uvspec radiative transfer model which is part of the freely available libRadtran toolbox [7] where it has been used frequently for spectral calculations and simulations of satellite channel responses. The gas absorption properties of LOWTRAN are based on HITRAN. Recent comparisons of measured thermal downward irradiances in the atmospheric window around 10 μm with LOWTRAN calculations have revealed some discrepancies, whereas high spectral resolution calculations using HITRAN 2004 [8] data show good agreement [9]. The commercially available MODTRAN code [10] also includes significantly improved spectral band parameterizations.

Buehler et al. [11] describe an approach for parameterizing gas absorption, where spectrally-integrated radiances are approximated by weighted means of radiances at so-called representative frequencies or wavelengths. The representative wavelengths together with their weights are selected by an optimization method which minimizes the deviation from the accurate spectrally-integrated radiances for a set of highly variable atmospheric states. Buehler et al. [11] focus on clear sky cases and parameterize thermal radiation channels of the HIRS satellite instrument. We developed a parameterization approach which is based on this work but includes adjustments to improve its applicability. For example, we added aerosols, water clouds, and ice clouds in the set of atmospheric states and increased the variability of the gas profiles. Furthermore, our approach determines automatically the number of representative wavelengths required to fulfill a parameterization accuracy threshold. Using this approach, we parameterized a large set of narrow spectral bands of different widths covering the thermal as well as the solar spectral range. Spectral response functions of many satellite channels were parameterized in addition (a list of channels is provided in Appendix A). We implemented the parameterized bands and channels, referred to as "REPTRAN" in the following, in the uvspec model [7]. The REPTRAN data files are available from the libRadtran webpage - http://libradtran.org.

In Section 2 we describe the representative wavelengths parameterization approach. After that, in Section 3, we apply the parameterization approach to spectral bands and satellite channels, investigate the spectral variability of the considered gas absorption, and compare results from parameterized bands and channels with results from exact high spectral resolution (HSR) calculations. We perform these comparisons for irradiances at the top of atmosphere, for which REPTRAN has been optimized, and also for irradiances at the surface and for heating rates as function of height. We also consider the LOWTRAN parameterization for the comparisons because it has been one of the mostly used absorption parameterizations of the uvspec model.

2. Methodology

2.1. Parameterization approach for spectral integrals

We parameterized spectrally-integrated radiative quantities by weighted means of these quantities at representative wavelengths, following the approach described by Buehler and coauthors [11] for broadband infrared radiometers.

Table 1: Parameters of aerosol and cloud layers in training set of atmospheres.

parameter	sampling	aerosol	water cloud	ice cloud
model		Mie	Mie	Key/Yang [13]
r_{eff}	log	0.1 - 10 μm	1 - 15 μm	habit-dependent
m_{r}	lin	1.28 - 2.00	-	-
m_{i}	log	0.001 - 0.1	-	-
z_{bottom}	lin	0 - 15 km	0 - 8 km	4 - 15 km
Δz		1 km	1 km	1 km
τ	log	0.1 - 2	1 - 20	1 - 20
# cases		420	168	168

The basic idea of the parameterization approach is given by

$$I_{\text{int}} = \int_{\lambda_{\min}}^{\lambda_{\max}} I(\lambda) R(\lambda) d\lambda \quad \approx \quad I_{\text{int,para}} = R_{\text{int}} \cdot \sum_{i_{\text{rep}}=1}^{n_{\text{rep}}} I(\lambda_{i_{\text{rep}}}) w_{i_{\text{rep}}} \tag{1}$$

$$\text{with} \qquad R_{\text{int}} = \int_{\lambda_{\min}}^{\lambda_{\max}} R(\lambda) d\lambda$$

The spectrally-integrated radiative quantity I_{int} is the integral of the spectral radiative quantity $I(\lambda)$ times the spectral weighting function $R(\lambda)$ (with $0 \leq R(\lambda) \leq 1$) from the limits $\lambda_{\min}$ to $\lambda_{\max}$ of the spectral interval. $R(\lambda)$ can describe, for example, an instrument channel response function or a wavelength band. I_{int} is approximated by $I_{\text{int,para}}$, which is the sum of the spectral radiative quantity I at n_{rep} representative wavelengths $\lambda_{i_{\text{rep}}}$ multiplied by their weights $w_{i_{\text{rep}}}$ and the term R_{int}. The sum over the weights $w_{i_{\text{rep}}}$ is equal to 1, thus the summation term of Eq. 1 is a weighted mean of the quantity I. The term R_{int} is a measure for the spectral width of the interval.

For each spectral interval, the set of representative wavelengths $\lambda_{i_{\text{rep}}}$ and weights $w_{i_{\text{rep}}}$ needs to be optimized. Our methodology is based on Buehler et al. [11] with some modifications as described below. The optimization approach uses spectrally high-resolved radiances of a set of different atmospheric states, the 'training set of atmospheres'.

2.1.1. Training set of atmospheres

Our aim is developing a parameterization approach which approximates wavelengths integrals for any realistic atmosphere of the Earth with low uncertainty. Thus, it is required that the variability present in the Earth's atmosphere is covered by the atmospheric profiles of the training data set. As a starting point, we selected the data set of Garand et al. [12] as used by Buehler et al. [11]: This data set includes 42 profiles of temperature, pressure, and volume mixing ratios of H_2O, O_3, CO_2, N_2O, CO, and CH_4. For O_2 and N_2 we assumed height-constant volume mixing ratios of 0.2095 and 0.7808, respectively. The top height of the profiles varies between 61 km and 67 km.

We investigated the variability of these 42 gas atmospheres and found that the variability of CO_2, N_2O, CO, and CH_4 does not cover the variability present in the Earth's atmosphere. Thus, we created for each of the 42 atmospheres a second gas atmosphere in which we halved the volume mixing ratios of one of CO_2, N_2O, CO, and CH_4 and doubled the volume mixing ratios of another one of these species, choosing the respective species randomly. Furthermore, the NO_2 profile from the US standard atmosphere is added to all 84 gas atmospheres.

We added cloud and aerosol layers to these gas atmospheres: For each gas atmosphere, one clear sky case, 5 aerosol cases, 2 water cloud cases, and 2 ice cloud cases are considered. Thus, the training data set consists of 840 different atmospheres. The microphysical properties of the aerosol and cloud particles and the heights of the layers were chosen randomly using either linear or logarithmic sampling according to the ranges given in Tab. 1. We considered a wide range of effective radii r_{eff}, layer bottom heights z_{bottom}, and optical thicknesses τ for both aerosols and clouds. In case of aerosols we considered also a wide range of wavelength-independent refractive indices $m = m_{\text{r}} + m_{\text{i}}\text{i}$. We fixed the widths of the log-normal aerosol size distributions to $\sigma = 2$. The water cloud droplet size distribution are gamma distributions with an effective variance of $v_{\text{eff}} = 0.1$. For the ice clouds we considered the

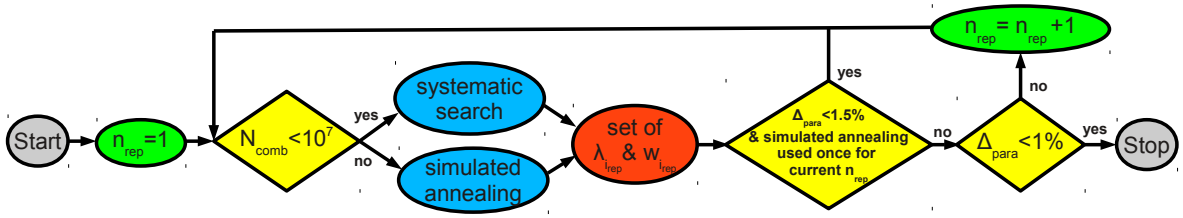

Figure 1: Flow chart for selection of representative wavelengths for a given spectral interval.

habits 'solid-column', 'hollow-column', 'rough-aggregate', 'rosette-6', 'plate', and 'droxtal' [13]. All aerosol and cloud layers have a vertical extent of $\Delta z = 1$ km.

2.1.2. High spectral resolution calculations

We performed high spectral resolution calculations for these atmospheres in the wavelength range from $\lambda \approx 395$ nm to $\lambda = 100\ \mu$m using a constant spectral resolution of 119.917 monochromatic calculations per cm^{-1}. This sampling rate corresponds to about $\Delta\lambda = 0.0002$ nm at $\lambda = 500$ nm and $\Delta\lambda = 0.0834$ nm at $\lambda = 10\ \mu$m, and a total of about 3 million wavelengths. The selected sampling rate is sufficient for the absorption in the lower atmosphere but may not sample all absorption features present in the upper atmosphere, where absorption lines can be quite narrow due to weak pressure broadening. However, such narrow absorption lines in the upper atmosphere typically are of little relevance for spectrally-integrated radiances or irradiances.

As the first step, the spectral absorption profiles of the 84 gas atmospheres (excluding the absorption data listed in subsequent paragraph) were calculated using the radiative transfer model ARTS [14]. The absorption was calculated from line parameters of the HITRAN 2004 spectroscopic database [8] for the above-mentioned eight gas species. MT_CKD (version 1.0) continuum absorption data [15] for H_2O, CO_2, N_2, and the collision-induced absorption by O_2 around $\lambda = 6.4\ \mu$m was added to the absorption profiles. Hitherto the ARTS model has not been applied in the visible spectral range.

Using the gas absorption profiles from ARTS, the DISORT radiative transfer solver [16], implemented in uvspec [7], was utilized to calculate the high spectral resolution radiances of the 840 atmospheres at their top. The calculations were performed for solar radiation using the Kurucz solar spectrum [17], as well as for thermal radiation. Uvspec adds the following gas absorption data to the gas absorption profiles calculated by ARTS: (a) O_3 absorption data from Molina [18] for $\lambda \leq 850$ nm, (b) collision-induced absorption by O_2 from Greenblatt [19] for $\lambda \leq 1.13\ \mu$m, and (c) absorption by NO_2 from Burrows [20] for $\lambda \leq 794$ nm. For each atmospheric state, the surface albedo as well as five cosines of viewing zenith angles were chosen randomly between 0 and 1. In case of solar radiation, two sun positions were considered with the cosines of the solar zenith angles chosen randomly between 0 and 1 and the relative azimuth angles (between observer and sun) chosen randomly between 0° and 180°. In total, $N_{\mathrm{rad}} = 8400$ and $N_{\mathrm{rad}} = 4200$ spectral radiances have been calculated for solar and thermal radiation, respectively.

2.1.3. Optimization of representative wavelengths

The representative wavelengths for each spectral interval are selected such that

$$\Delta_{\mathrm{para}} = \sqrt{\frac{1}{N_{\mathrm{rad}}} \sum_{i_{\mathrm{rad}}=1}^{N_{\mathrm{rad}}} \left(\frac{I_{\mathrm{int,para,i_{rad}}} - I_{\mathrm{int,i_{rad}}}}{I_{\mathrm{int,i_{rad}}}} \right)^2} \tag{2}$$

is below 1%. Δ_{para} is the root mean square relative deviation of the parameterized radiances $I_{\mathrm{int,para}}$ w.r.t. the training data set.

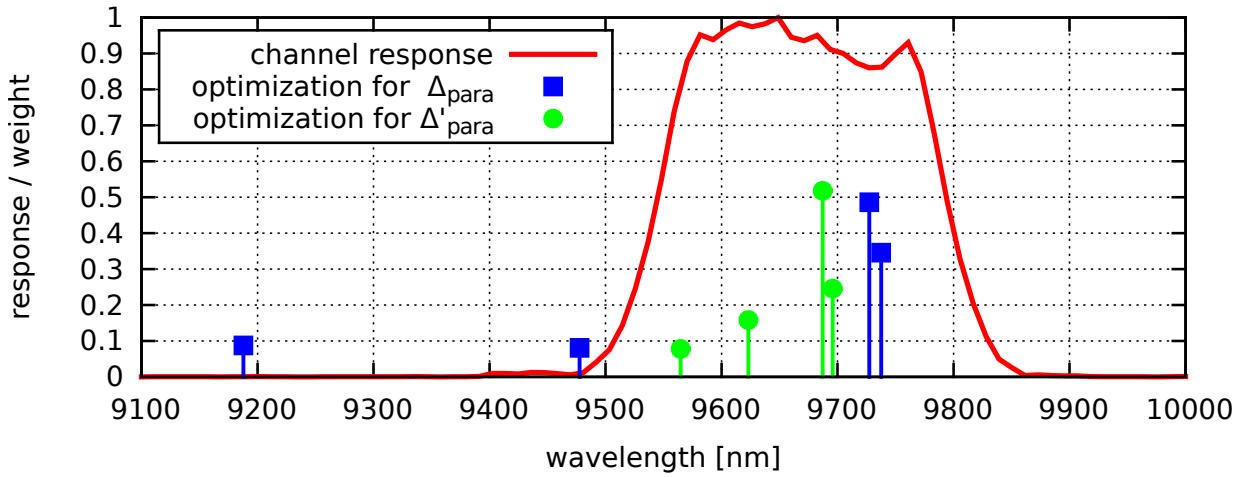

Figure 2: Response function (red line) of Meteosat Second Generation infrared channel around $\lambda = 9.7\ \mu$m; the blue boxes show representative wavelengths optimized for small Δ_{para}, whereas the green circles show representative wavelengths optimized for small Δ'_{para}; the weigth of each representative wavelength can be read from the vertical axis.

A flow chart of the selection procedure is shown in Fig. 1. The selection starts with the number of representative wavelengths n_{rep} set to 1, and n_{rep} is increased until Δ_{para} has fallen below the 1% threshold. All n_{hsr} wavelengths from the high spectral resolution calculations in the range λ_{min} to λ_{max} are candidates for representative wavelengths. For a given number of representative wavelengths n_{rep}, the representative wavelengths are optimized using two different approaches: If the number of possible wavelengths combinations N_{comb}, which is given by

$$N_{\text{comb}} = \left(\begin{array}{c} n_{\text{hsr}} \\ n_{\text{rep}} \end{array} \right) \tag{3}$$

is below 10^7, the optimum combination is searched systematically. If N_{comb} is larger, the systematic search becomes impractical and the wavelengths combination is optimized using simulated annealing as described by Buehler et al. [11]. Simulated annealing not necessarily finds the absolute optimum wavelengths combination for a given n_{rep}; thus, a second simulated annealing run with the same n_{rep} is performed if $\Delta_{\text{para}} < 1.5\%$ was achieved by simulated annealing. We increase n_{rep} by 1 in any other case if $\Delta_{\text{para}} < 1\%$ was not achieved.

When determining the representative wavelengths optimizing for small Δ_{para} (Eq. 2) we found that often wavelengths were selected where the spectral response function is small. An example is shown in Fig. 2 where the blue boxes illustrate the wavelengths $\lambda_{i_{\text{rep}}}$ and their weights selected for a spectral response function $R(\lambda)$ of a MSG2 infrared channel (red line). Representative wavelengths with low $R(\lambda_{i_{\text{rep}}})$ can reduce the robustness of the approach in particular if an atmospheric constituent with a strong spectral variability that has not been considered in our training data set is modeled. To punish the selection of such wavelengths we defined Δ'_{para} which adds an extra factor to Δ_{para}:

$$\Delta'_{\text{para}} = \Delta_{\text{para}} \cdot \left(1 + \sqrt{\frac{1}{n_{\text{rep}}} \sum_{i_{\text{rep}}=1}^{n_{\text{rep}}} \left(\frac{w_{i_{\text{rep}}}}{R(\lambda_{i_{\text{rep}}})} \right)^2} \right). \tag{4}$$

Our approach optimizes the wavelengths combination for small Δ'_{para} during the systematic search and during simulated annealing (Fig. 1). The effect of optimizing for small Δ'_{para} instead of small Δ_{para} is illustrated by Fig. 2: when comparing the blue boxes with the green circles it becomes clear that optimizing for Δ'_{para} (green circles) generates representative wavelengths only where $R(\lambda)$ is not small. The weights $w_{i_{\text{rep}}}$ for a given wavelengths combination are always determined using a nonnegative least squares routine that optimizes for small Δ_{para}.

2.2. Parameterized spectral intervals

We applied this parameterization approach to narrow spectral bands and to spectral response functions of satellite instrument channels in the solar and thermal spectral range. To create the sets of spectral bands, we divided the wavelength spectrum into adjacent non-overlapping bands with three different widths: A coarse case with band widths of 15 cm^{-1}, a medium case with 5 cm^{-1}, and a fine case with 1 cm^{-1}. We consider solar radiation in the range from $\lambda \approx 395$ nm (25315 cm^{-1}) to $\lambda \approx 5025$ nm (1990 cm^{-1}), which results in 1555, 4665, or 23325 bands, depending on the band widths. For radiation from thermal emission, the range from $\lambda = 2.5\ \mu$m (4000 cm^{-1}) to $\lambda = 100\,\mu$m (100 cm^{-1}) is covered by 260, 780, or 3900 bands, depending on the band widths. The spectral weight $R(\lambda)$ of a band from $\lambda_{\min}$ to $\lambda_{\max}$ is defined as $R(\lambda) = 1$ for $\lambda \in [\lambda_{\min}, \lambda_{\max}]$. In addition to these spectral bands, we have parameterized spectral response functions of almost 400 channels of instruments on the ADEOS, ALOS, EarthCARE, Envisat, ERS, Landsat, MSG, PARASOL, Proba, Sentinel, Seosat, and SPOT satellites (a list of channels is provided in Appendix A). We have implemented the parameterized bands and satellite instrument channels in the uvspec radiative transfer model.

2.3. Absorption lookup tables

The absorption cross sections C_{abs} of gas molecules at the representative wavelengths are required for the application of the parameterized spectral intervals in radiative transfer calculations. Following the approach of Buehler et al. [21], lookup tables of pre-calculated absorption cross sections are used to provide the required data to the uvspec model. The lookup tables contain absorption cross sections of H_2O, O_3, CO_2, N_2O, CO, CH_4, O_2, and N_2 on a grid of pressures p and temperatures T. The water vapour absorption also depends on the water vapour mixing ratio x_{H_2O}. The cross sections were calculated using the ARTS model based on HITRAN 2004 line data [8] together with MT_CKD absorption continua [15] for H_2O, CO_2, N_2, and O_2 (same data as described in Sect. 2.1.2). The grid of p, T, and x_{H_2O} is modified compared with the 'wide' setup described by [21]: the spacing of the p grid, in terms of log p, is less dense at high altitudes than at low altitudes, which is justified by comparatively low gas abundances at high altitudes; we use 41 p grid points, from 110000 Pa to 0.0007 Pa with a step of $2^{-0.25}$ from 110000 Pa to 46249 Pa, then $2^{-0.5}$ till 90 Pa, and finally 1/2 for lower pressures. The temperature T at each pressure level p is perturbed relative to the temperature of the US standard atmosphere [22] by 0 K, ±20 K, ±40 K, ±70 K, and ±120 K. For water vapour, cross sections are calculated for mixing ratios $x_{H_2O} = 0$, 0.02, 0.05, and 0.10.

We converted the lookup tables of absorption cross sections from ARTS to a format readable by uvspec. In order to reduce the file sizes, the converted lookup tables consist of one file per species and consider only representative wavelengths where the species absorbs. For calculating the absorption cross sections of the gas molecules at the p, T, and x_{H_2O} of interest, uvspec applies linear interpolation between the grid points of the lookup tables. Alongside with the cross sections from the lookup tables, uvspec considers also the independent absorption data for $\lambda \leq 1130$ nm which we described above for the high spectral resolution calculations; that is absorption by O_3 [18], by O_2 [19], and by NO_2 [20].

3. Results and discussion

In this section we first describe the application of the representative wavelengths parameterization approach and examine the spectral variability of the absorption of the considered gas species. Then we compare, for validation purposes, the radiative transfer modeling results of the parameterized satellite channels and spectral bands (REPTRAN) with respective results from high spectral resolution (HSR) calculations for various atmospheric states. These comparisons are performed not only at the top of atmosphere, for which REPTRAN has been optimized, but also for irradiances at the surface and for atmospheric heating rates. Results from the LOWTRAN parameterization are also considered for the comparisons because LOWTRAN has been used frequently for radiative transfer simulations in wavelength regions affected by gas absorption.

3.1. Parameterization application

The black curves in Fig. 3 show average relative errors Δ_{para} of the parameterized coarse resolution bands in percent as function of wavelength. The scales of the wavelength axes in Fig. 3 (and most subsequent figures) are constant in terms of wavenumbers, so that the bands are equidistant. The upper panel shows the parameterization

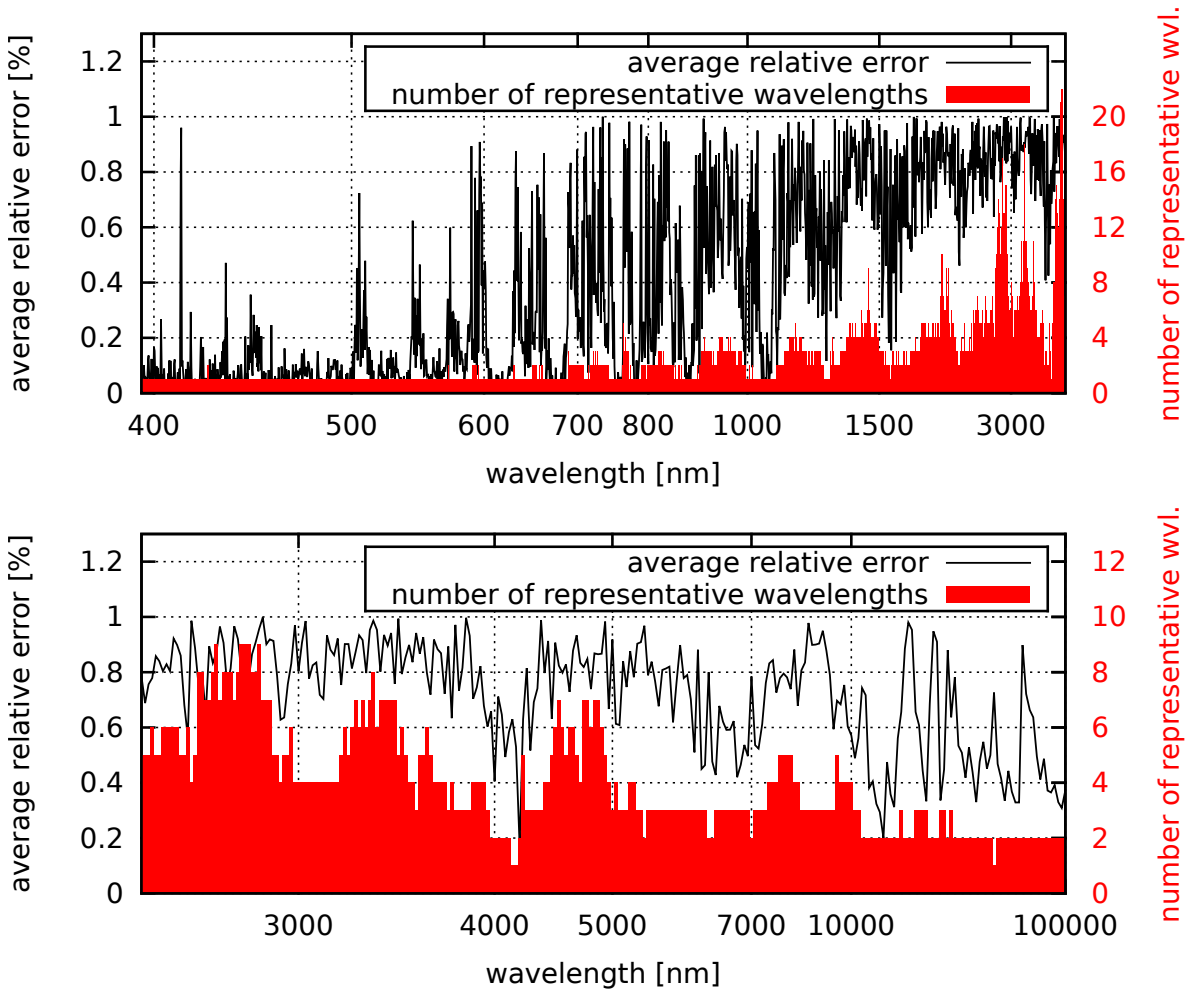

Figure 3: Average relative parameterization error Δ_{para} of coarse resolution bands (black lines) and number of representative wavelengths n_{rep} per coarse resolution band (red bars); the upper panel shows the data of the parameterized solar bands whereas the lower panel shows the data of the parameterized thermal bands; the scales of the wavelength axes are constant in terms of wavenumbers.

errors for solar radiation, whereas the lower panel shows the errors for thermal source. As mentioned in the previous section, Δ_{para} has been calculated for the radiances at the top of atmosphere of the training data set and $\Delta_{\text{para}} < 1\%$ was used as threshold for each parameterized band. The black curves reveal that Δ_{para} is significantly smaller than 1% for bands in which the absorption by gases is weak, e.g. at most visible wavelengths.

The red bars in Fig. 3 illustrate n_{rep}, the number of representative wavelengths of each parameterized coarse resolution band (numbers on the right vertical axis). n_{rep} increases with the strength and the spectral variability of the absorption by gases and with increasing number of relevant gas species. Only one representative wavelength is required to approximate band-integrals with average relative errors of about 0.1% for many bands at visible wavelengths where absorption is either weak or smooth (see upper panel of Fig. 3).

For wavelengths larger than about 2.5 μm often $n_{\text{rep}} > 10$ is required in case of solar radiation. A reason for this comparatively large n_{rep} is the large number of absorption lines of several gas species in this spectral region. In case of thermal radiation (lower panel), however, n_{rep} is always lower than 10, even in the overlap region between both radiation sources (2.5 μm to 5.0 μm). The reason for the difference of n_{rep} in this overlap region is that the spectral variability of the thermal emission is either weak (for emission by the surface or by atmospheric particles) or correlated with the spectral variability of the absorption by gases (for emission by gases), whereas we can assume that the Fraunhofer lines of the solar spectrum are not correlated with the absorption by gases in the Earth's atmosphere.

Fig. 4 compares the three spectral resolutions of the sets of parameterized bands around $\lambda \approx 760$ nm where absorption by O_2 (so-called O2A-band, upper panel) is significant and in a thermal range between 6.0 to 6.4 μm (lower panel) where water vapour is a strong absorber. Both plots show upward irradiances at top of the US standard atmosphere [22] with the surface albedo set to 0.3. The irradiances in the lower panel have been converted to brightness temperatures. The plots clearly illustrate that the coarse resolution bands smooth away the strong variability of the fine resolution bands.

Table 2: Number of representative wavelengths for all spectral intervals / total number of spectral intervals / average number of representative wavelengths per spectral interval ($\overline{n_{\text{rep}}}$) for the different sets of parameterized spectral intervals.

sets of spectral intervals	solar	thermal
coarse bands, 15 cm^{-1} width	3695 / 1555 / 2.38	1037 / 260 / 3.99
medium bands, 5 cm^{-1} width	10409 / 4665 / 2.23	2813 / 780 / 3.61
fine bands, 1 cm^{-1} width	45071 / 23325 / 1.93	12134 / 3900 / 3.11
satellite channels	720 / 351 / 2.05	155 / 42 / 3.69

Tab. 2 shows the total number of representative wavelengths, the total number of spectral intervals (bands or channels), as well as the average number of representative wavelengths per spectral interval, $\overline{n_{\text{rep}}}$, for the different sets of spectral intervals on which we applied our parameterization approach. The total number of representative wavelengths increases with increasing spectral resolution by a factor of ≈12 from coarse to fine resolution whereas the number of bands increases by a factor of 15. As a consequence, the average $\overline{n_{\text{rep}}}$ decreases from 3.99 for coarse resolution thermal bands to 3.11 for the fine resolution thermal bands. $\overline{n_{\text{rep}}}$ is lower for the solar bands where it decreases from 2.38 for coarse resolution bands to 1.93 for fine resolution bands.

Table 3: Computation time (CPU time) required for simulating top of atmosphere irradiances with TWOSTREAM / radiances with DISORT (16 streams) of all parameterized bands of the different resolutions; for comparison, high spectral resolution calculations (HSR) covering the same spectral range; measured on a Intel Xeon E5-2650 CPU for complete uvspec runs including initialization.

method	solar	thermal
REPTRAN coarse	1.9 s / 15.7 s	0.5 s / 4.2 s
REPTRAN medium	6.0 s / 44.7 s	1.4 s / 11.6 s
REPTRAN fine	33.3 s / 199 s	6.9 s / 50.6 s
HSR with 40λ per cm^{-1} and pre-calculated gas absorption profiles	189 s / 3587 s	36.4 s / 613 s

Tab. 3 summarizes the computation time required for the application of the REPTRAN bands on the US standard

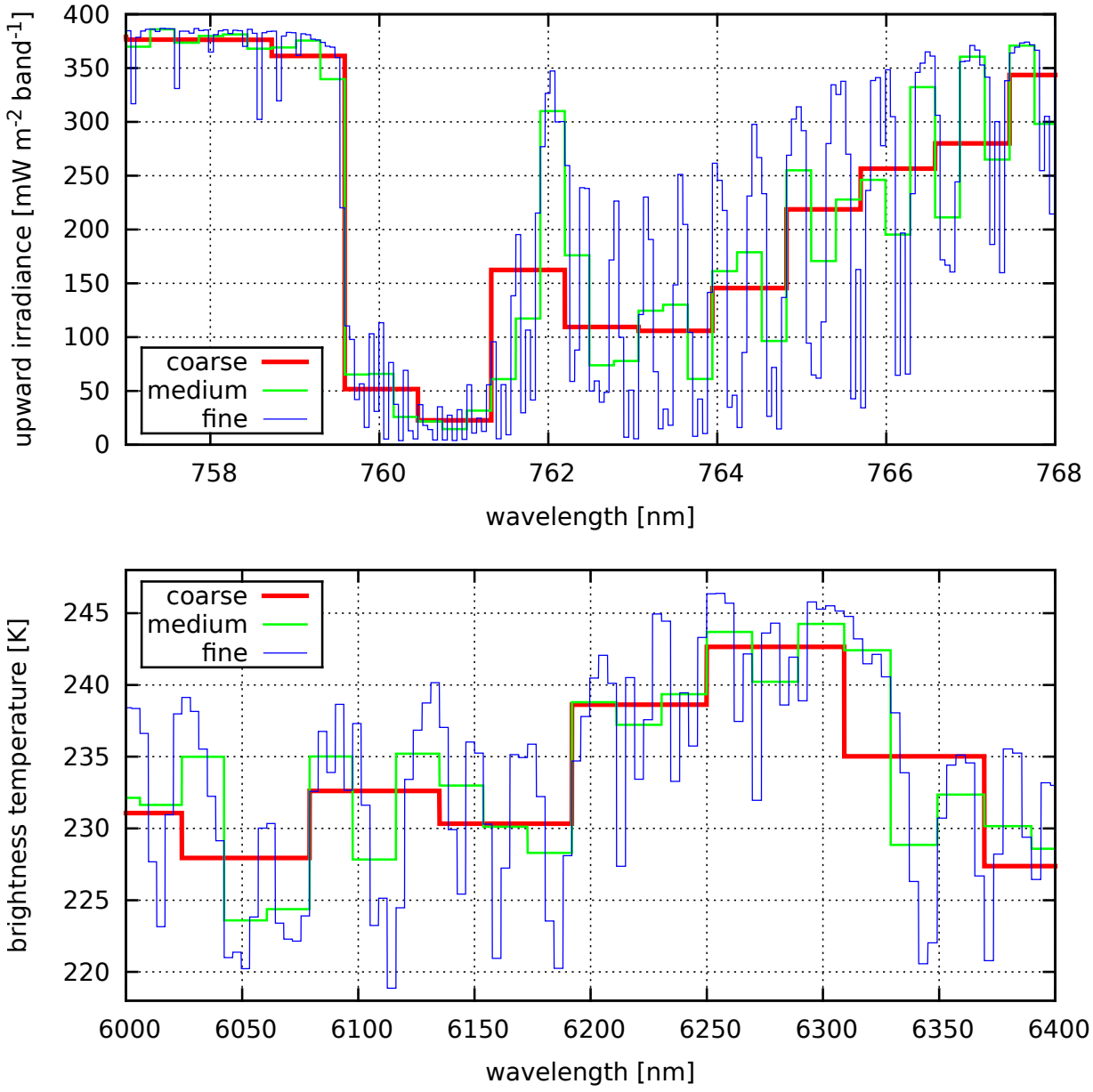

Figure 4: Comparison of spectral resolutions of the parameterized bands around the O2A absorption band (upper panel) and a thermal range (lower panel).

atmosphere [22] without aerosol or clouds and the complete spectral range they have been created for. The computation times are for complete uvspec runs, including initialization etc. The REPTRAN bands have been applied for the simulation of top of atmosphere irradiances using the TWOSTREAM solver [23] and top of atmosphere radiances using the DISORT solver [16]. For comparison, high spectral resolution calculations (HSR) have been performed on the same spectral range using a spectral resolution of 40 monochromatic simulations per cm^{-1}. The absorption coefficients for the HSR calculations have been calculated using ARTS (computation times of ARTS not considered in Tab. 3) and were then used as input to the uvspec model for simulating the irradiances and radiances. Simulating irradiances within all coarse resolution solar bands (15 cm^{-1} width) from 395 nm to 5000 nm requires 1.9 s of computation time (single-threaded) on a Intel Xeon E5-2650 CPU; the computational cost increases with increasing spectral resolution, approximately proportionally with the number of bands. The computational cost increases by a factor of 6 to 8 when radiances are simulated instead of irradiances. In case of HSR calculations with 40 lines per cm^{-1}, the computation time requirement increases by a factor of about 5 to 20 compared with the fine resolution REPTRAN bands if the spectral absorption coefficients have been pre-calculated. The computation time requirement for simulations of the thermal bands is approximately one quarter of the requirement for the solar bands. The reduction of computation time for REPTRAN as compared with HSR, which can be up to several orders of magnitude, mainly depends on the selected spectral resolutions of REPTRAN and HSR and whether the gas absorption coefficients are already available for HSR calculations or are yet to be calculated.

The average value of n_{rep} over all parameterized satellite instrument channels is about 2 for solar source and 3.7 for thermal source (Tab. 2). The low number of radiative transfer calculations required to simulate channel-integrated radiances results in very low computational times for the parameterized channels. For example, a uvspec simulation of radiances at the parameterized 3.9 μm channel of SEVIRI ($n_{\mathrm{rep}} = 8$), using the DISORT solver and thermal radiation, takes 0.105 s on a PC. Using the LOWTRAN parameterization with a spectral resolution of 5 cm^{-1} takes 9.1 s for the same channel.

3.2. Absorption by gas species

Direct transmittances of different gas species considered by uvspec are shown in Fig. 5 as function of wavelength. Here, the transmittance of a species is the fraction of the incoming sunlight (with the sun at zenith) that passes through the US standard atmosphere [22] to the surface; all other species are removed from the atmospheric setup. Scattering is switched off. Note the reversed logarithmic scale for '1 - transmittance', i.e. the absorbed fraction of the incident light, on the vertical axes in Fig. 5. The upper panel shows the data for $\lambda < 850$ nm, whereas the lower panel shows the data for $\lambda > 850$ nm. The data has been calculated using the parameterized solar coarse resolution bands with the absorption calculated as described in Sect. 2.3. Water vapour absorption (red) is significant in most bands in the near infrared; absorption by O_2 is significant mainly in the O2A band around $\lambda = 760$ nm. The lower panel shows that absorption by CO_2 and CH_4 becomes increasingly relevant for about $\lambda \geq 1.4$ μm.

Fig. 6 shows the transmittance of the different species of the US standard atmosphere calculated using the parameterized thermal coarse resolution bands. The upper panel of Fig. 6 shows transmittances for the main absorbers, whereas the lower panel shows data for the minor absorbers. The absorption by water vapour (red line in upper panel of Fig. 6) is strong (virtually no transmittance) in large parts of the thermal spectrum, except from about 3.4 μm to 4.8 μm and from about 8 μm to 15 μm. Within these wavelength ranges, absorption by CO_2, and to a minor extent also absorption by CH_4, O_3, N_2O, N_2, and CO is relevant.

3.3. Parameterized satellite channels

We have applied the REPTRAN parameterization approach to almost 400 satellite channels (Appendix A). The parameterization data ($\lambda_{i_{\mathrm{rep}}}$ and $w_{i_{\mathrm{rep}}}$) for the channels of the Spinning Enhanced Visible and Infrared Imager (SEVIRI) on the MSG3 satellite is provided in Appendix B. For validation of REPTRAN, we now compare modeling results for the parameterized MSG3 channels with respective results from HSR calculations.

Tab. 4 shows mean (maximum) deviations of the parameterized channels from HSR calculations for radiances at top of atmosphere. Four solar channels of SEVIRI are considered. The deviations were averaged over 12 atmospheres and 10 viewing directions (cosines of viewing zenith angle equidistant from 0.1 to 1.0) for each atmosphere. The 12 atmospheres did not contain aerosols nor clouds and the sun is at zenith. The atmospheric set included 6 standard atmospheres [22] and 6 randomly chosen atmospheres from an ECMWF data set that has been optimized for large

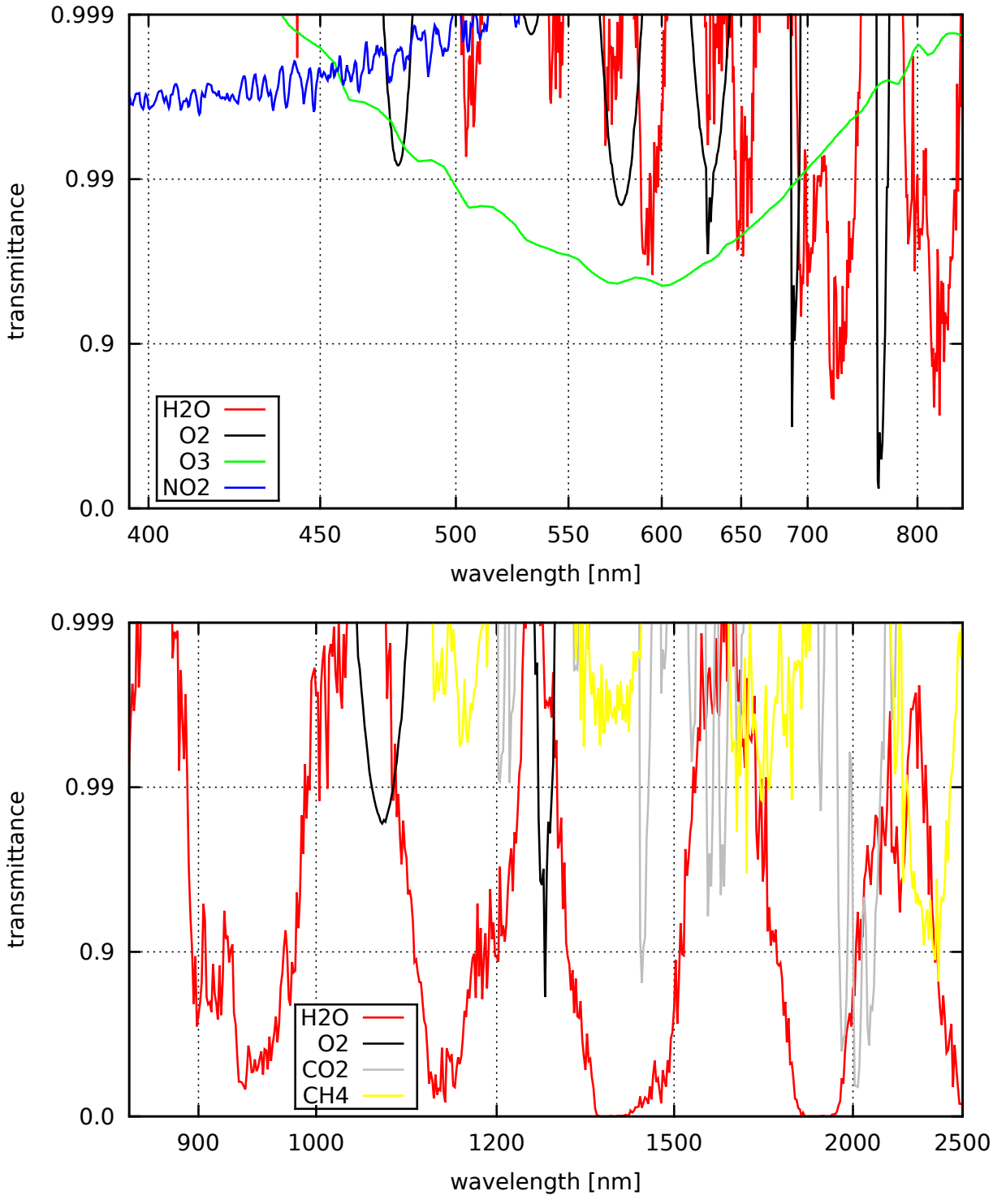

Figure 5: Transmittance of absorbing species through the US standard atmosphere from λ = 395 nm to 850 nm (upper panel) and 850 nm to 2500 nm (lower panel), calculated using the parameterized solar coarse resolution bands; for clarity, the transmittance of O_3, N_2O, and CO is not shown is the lower panel, though it is between 0.999 and 0.99 for some bands (and > 0.999 elsewhere).

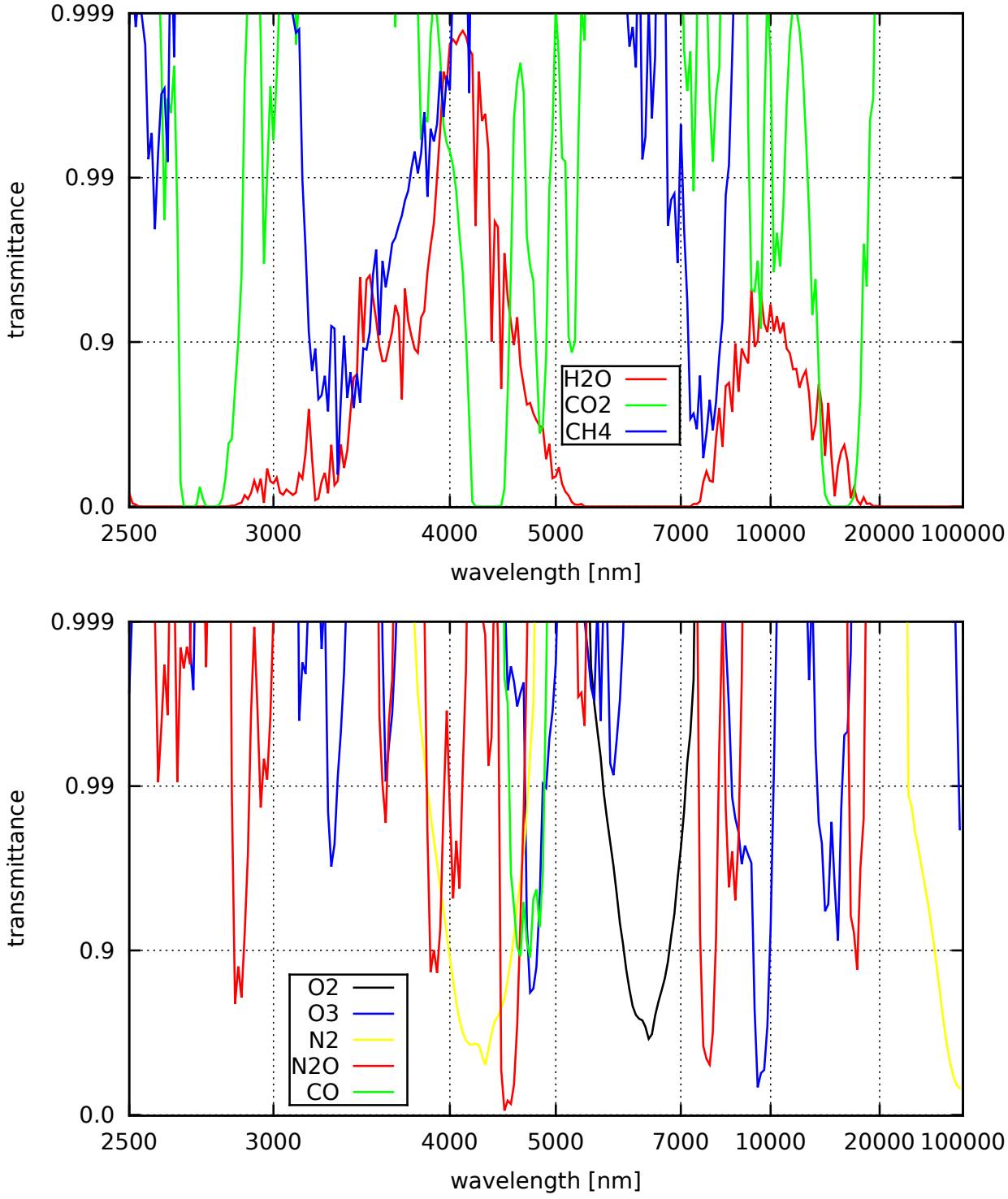

Figure 6: Analogous to Fig. 5, but for thermal bands.

Table 4: Root mean squared relative deviations (maximum) of radiances within solar satellite channels, averaged over 10 viewing angles and 12 atmospheres (see text for details); the surface albedo is set to 0.3.

channel	REPTRAN - HSR	LOWTRAN - HSR
msg3_seviri_ch006	0.30% (0.68%)	0.96% (1.43%)
msg3_seviri_ch008	0.44% (1.62%)	1.79% (7.64%)
msg3_seviri_ch016	0.51% (1.09%)	4.02% (18.3%)
msg3_seviri_ch039	0.35% (1.28%)	9.93% (47.1%)

Table 5: Root mean squared deviations (maximum) for radiance brightness temperatures within thermal satellite channels, averaged over 10 different viewing angles and 12 atmospheres (see text for details); the surface albedo is set to 0.0.

channel	REPTRAN - HSR	LOWTRAN - HSR
msg3_seviri_ch039	0.10 K (0.31 K)	0.50 K (1.59 K)
msg3_seviri_ch062	0.21 K (0.82 K)	0.57 K (0.92 K)
msg3_seviri_ch073	0.27 K (0.76 K)	1.87 K (2.90 K)
msg3_seviri_ch087	0.22 K (0.45 K)	0.40 K (1.17 K)
msg3_seviri_ch097	0.35 K (0.78 K)	2.08 K (7.51 K)
msg3_seviri_ch108	0.09 K (0.23 K)	0.40 K (1.14 K)
msg3_seviri_ch120	0.17 K (0.31 K)	0.50 K (1.22 K)
msg3_seviri_ch134	0.39 K (0.96 K)	3.76 K (7.15 K)

variability of temperature [24]. The N_2, N_2O, CH_4, and CO mixing ratio profiles from the US standard atmosphere were used in all 12 atmospheres. Rayleigh scattering and a surface albedo of 0.3 were considered in all simulations for Tab. 4. The high spectral resolution calculations (HSR) for each channel were performed at 12200 wavelengths within the channel boundaries. A spectral resolution of 1 nm was used for the LOWTRAN calculations.

The average relative deviation of REPTRAN from HSR is lower than 1% for all channels when averaged over the 12 atmospheres and 10 viewing directions, with a maximum deviation of 1.62%. The deviations of LOWTRAN from HSR are significantly larger with average values between 1% and 10%. Large deviations are found for the 3.9 μm channel both for the standard and the ECMWF atmospheres, with a maximum value of 47% for the tropical atmosphere at high viewing zenith angle.

For eight thermal channels of SEVIRI, mean (maximum) deviations of brightness temperatures at top of atmosphere are given in Tab. 5. The mean deviations of the brightness temperatures of REPTRAN from exact HSR calculations are between 0.09 K and 0.39 K, depending on the channel, with a maximum deviation of 0.96 K for the 13.4 μm channel. The mean deviations of LOWTRAN from HSR are between 0.40 K and 3.76 K with a maximum deviation of 7.51 K for the 9.7 μm channel. The deviations of LOWTRAN from HSR are a factor of about 2 to 9 larger than the deviations of REPTRAN from the exact method. We point out that REPTRAN satellite channels require a very low number of monochromatic radiative transfer calculations (on average 2-4, see Tab. 2) which results in a very low computation time for which an example was already given in Sect. 3.1.

3.4. Parameterized bands applied for top of atmosphere irradiances

We model top of atmosphere irradiances using REPTRAN bands and compare these irradiances with equivalent band-integrated irradiances from exact HSR calculations. As described above, the REPTRAN approach has been optimized for radiances at the top of atmosphere. The simulations evaluated in the following consider also atmospheres which were not considered by the training data set; most atmospheric parameters, however, are within the range spanned by the training data set. We apply the parameterized coarse resolution bands, which are characterized by a spectral width of 15 cm^{-1}. In case of HSR, the simulations are performed analogous to those performed for the training data set (Sect. 2.1.2), except that we increased the spectral resolution by about 50% to 180 per cm^{-1} in order to test also the sufficiency of the spectral resolution we used for our training data set. LOWTRAN is considered using

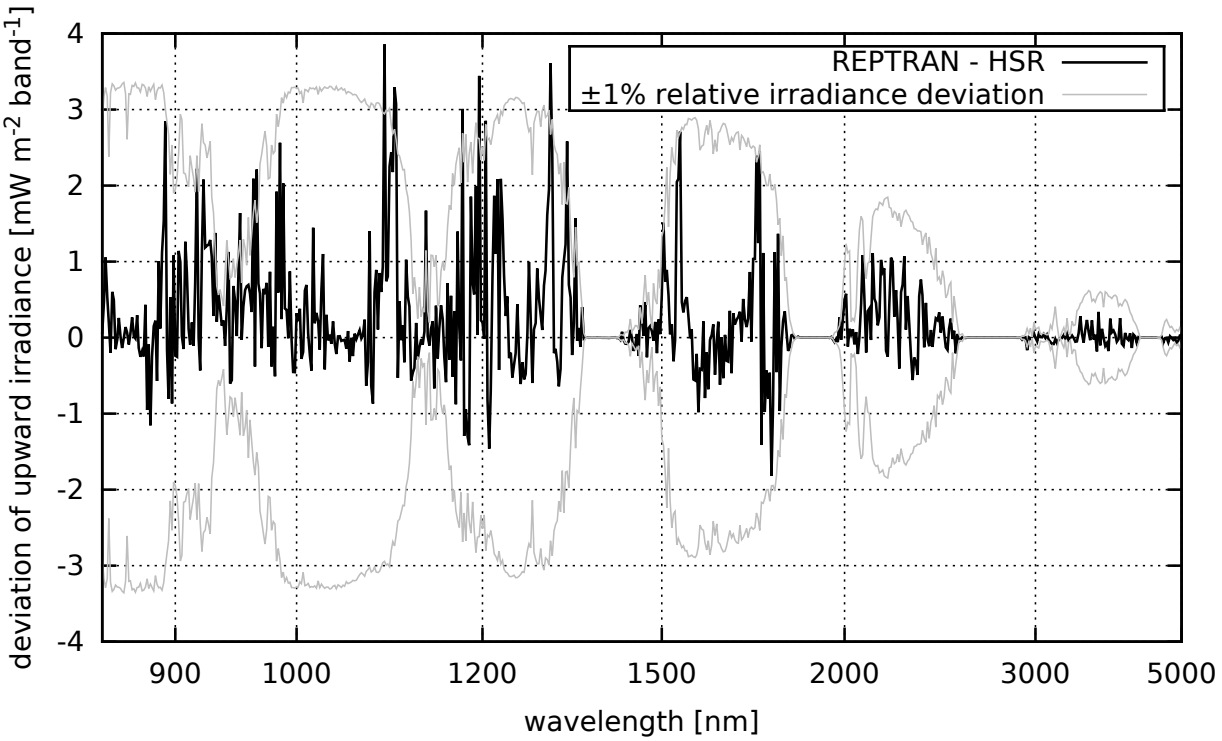

Figure 7: Deviations of the upward irradiances at top of the US standard atmosphere of the parameterized solar bands from high spectral resolution calculations (black line); surface albedo is set to 0.3.

a spectral resolution of 1 per cm^{-1} for the radiative transfer calculations and using, for solar bands, the full resolution solar spectrum from Kurucz [17].

3.4.1. Solar bands

We compare the upward irradiance at top of atmosphere modeled in the solar spectral range using the different methods. First, we investigate results for the US standard atmosphere [22] without clouds or aerosols. The deviation of the upward irradiance of REPTRAN bands from HSR calculations for this atmosphere is shown for $\lambda \geq 850$ nm as the black line in Fig. 7. The surface albedo is set to 0.3. The thin gray lines illustrate, for comparison, absolute deviations for 1% relative deviation from the absolute irradiances. Bands with strong gas absorption are characterized by low absolute irradiances thus the distance between both gray lines is small for such bands. For example, the water vapour absorption band around $\lambda = 950$ nm is clearly visible for the gray lines in Fig. 7. The deviations of REPTRAN results from the exact HSR calculations are small with maximum values of less than 4 mW m^{-2} $band^{-1}$. The comparisons of the black line with the gray lines shows that the relative error of the parameterization is below 1% for most bands.

Tab. 6 shows mean and maximum deviations between REPTRAN and HSR for top of atmosphere upward irradiances from the same atmospheres as in Sect. 3.3. The wavelength range from 395 nm to 5 μm is considered using the coarse band resolution. Tab. 6 reveals that the deviations of REPTRAN bands from the exact HSR calculations are of comparable magnitude for all investigated atmospheres. This is a strong indication that our training data set is sufficient to cover a wide range of atmospheric states. The deviations of LOWTRAN, also shown in Tab. 6, are more than one order of magnitude larger than the deviations of REPTRAN, independent of the atmospheric state.

The uncertainties of transmittances, i.e. the ratios between the upward irradiances and the incoming solar irradiances, calculated using the REPTRAN bands (not shown) are higher than the uncertainties of the upward irradiances. The reason for the increased uncertainty of transmittances is that the representative wavelengths were not directly optimized for an accurate parameterization of the incoming solar irradiance. The root mean squared relative devia-

Table 6: Root mean squared (maximum) deviations between the calculation methods for upward irradiances at top of different atmospheres [22, 24] for solar coarse bands in the spectral range from 395 nm to 5 μm; the unit is mW m^{-2} band^{-1}; surface albedo is set to 0.3.

atmosphere	REPTRAN - HSR	LOWTRAN - HSR
US standard	0.588 (3.86)	11.5 (97.1)
subarctic winter	0.615 (4.68)	10.6 (98.9)
subarctic summer	0.553 (3.01)	12.0 (96.7)
midlatitude winter	0.581 (5.00)	11.1 (98.3)
midlatitude summer	0.577 (3.30)	12.6 (96.3)
tropical	0.622 (3.60)	13.3 (96.3)
6 ECMWF atmospheres	0.696 (5.39)	10.1 (98.9)

tion between REPTRAN and HSR for the band-integrated incoming solar irradiances is on the order of 1.3% with a maximum deviation of 13.8%. The relative deviations for transmittances are of comparable magnitude.

3.4.2. Thermal bands

Before we compare REPTRAN with other methods in the thermal spectral range, we investigate two sources for deviations: First, differences in the model layer optical depth calculations are relevant when comparing top of atmosphere irradiances in the thermal range. For example, the data of the standard atmospheres [22] is available at a 5 km height resolution for heights above 50 km, thus model layers are 5 km thick. In case of high spectral resolution calculations (HSR), we calculate the gas absorption profiles with ARTS and use them in uvspec. For export to uvspec, the current version of ARTS uses

$$\tau_{\mathrm{HSR}} = \frac{C_{\mathrm{abs}}(z_{\mathrm{top}}) \cdot n(z_{\mathrm{top}}) + C_{\mathrm{abs}}(z_{\mathrm{bottom}}) \cdot n(z_{\mathrm{bottom}})}{2} \cdot (z_{\mathrm{top}} - z_{\mathrm{bottom}}) \tag{5}$$

to calculate the layer optical depth for each gas species and model atmosphere layer from z_{bottom} to z_{top}. In case of REPTRAN and LOWTRAN, by default the following formula is used by uvspec:

$$\tau_{\mathrm{uvspec}} = \frac{C_{\mathrm{abs}}(z_{\mathrm{top}}) + C_{\mathrm{abs}}(z_{\mathrm{bottom}})}{2} \cdot \frac{n(z_{\mathrm{top}}) + n(z_{\mathrm{bottom}})}{2} \cdot (z_{\mathrm{top}} - z_{\mathrm{bottom}}) \tag{6}$$

Here, C_{abs} is the absorption cross section (depending on p, T, $x_{\mathrm{H_2O}}$) at height z, and n the number density of the gas species at height z. Fig. 8 illustrates the brightness temperature deviations due to the difference between both formulas for top of atmosphere upward irradiances. The deviation due to the different formulas is larger than 0.1 K for many bands, reaching values up to 0.3 K. The thin gray lines illustrate the deviation of the brightness temperature when the irradiance deviates by ±1%. Comparison of the black and gray lines shows that the relative deviation of the irradiance is on the order of 2% for $\lambda < 3$ μm and 1% or smaller elsewhere. To exclude deviations due to different layer optical depth formulas, we perform the REPTRAN and LOWTRAN calculations using Eq. 5 instead of the default Eq. 6 in the remainder of this section.

A second source for deviations is the fact that the training data set used for parameterizing the bands consists of atmospheres with top heights around 65 km, but the heights of the standard atmospheres [22], which are included in the libRadtran package and used in the current section, are 120 km. The pressure and temperature conditions at $z > 65$ km may result in spectral absorption features that were not considered when parameterizing the spectral bands. Fig. 9 compares the deviation of REPTRAN from HSR for the US standard atmosphere with a top height of 120 km (black) and the same atmosphere cut at a height of 60 km (green). This "top height effect" is relevant at wavelengths were the green line is visible in this figure. These wavelengths are characterized by non-negligible gas absorption at the high altitudes. Absorption by CO_2 is relevant at around 2.7 μm, 4.3 μm and 15 μm, whereas absorption by O_3 and H_2O is relevant at the other spectral regions where the green line is visible in Fig. 9. While the maximum deviation of REPTRAN from HSR is slightly larger than 0.5 K when the height of the atmosphere is only 60 km, the maximum deviation increases to about 1 K (or about 5% of the irradiance) when the height of the atmosphere is 120 km. This "top height effect" is not compensated in the following since we use the complete atmospheric profiles (extending to heights of 120 km for all standard atmospheres and about 78 km for the ECMWF atmospheres).

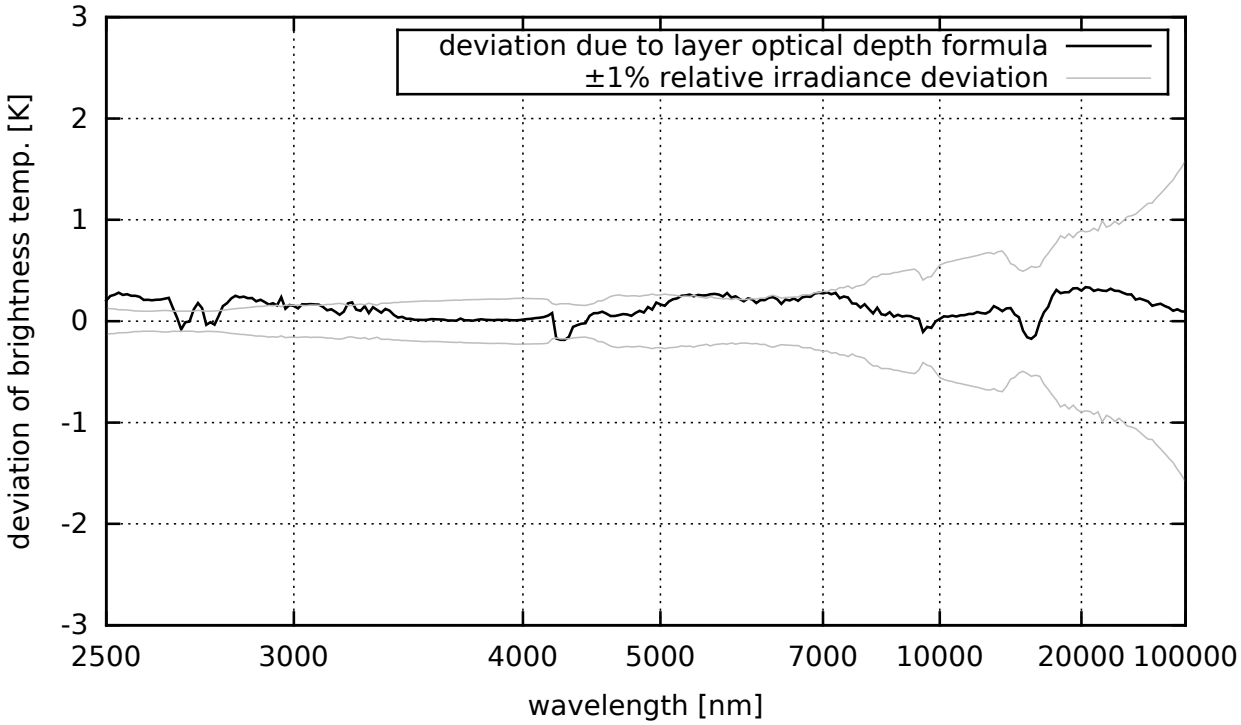

Figure 8: Deviations of brightness temperatures of upward irradiances at the top of the US standard atmosphere due to different layer optical depth formulas [Eq. 5 vs. Eq. 6] using REPTRAN thermal bands (black line); the surface albedo is set to 0.

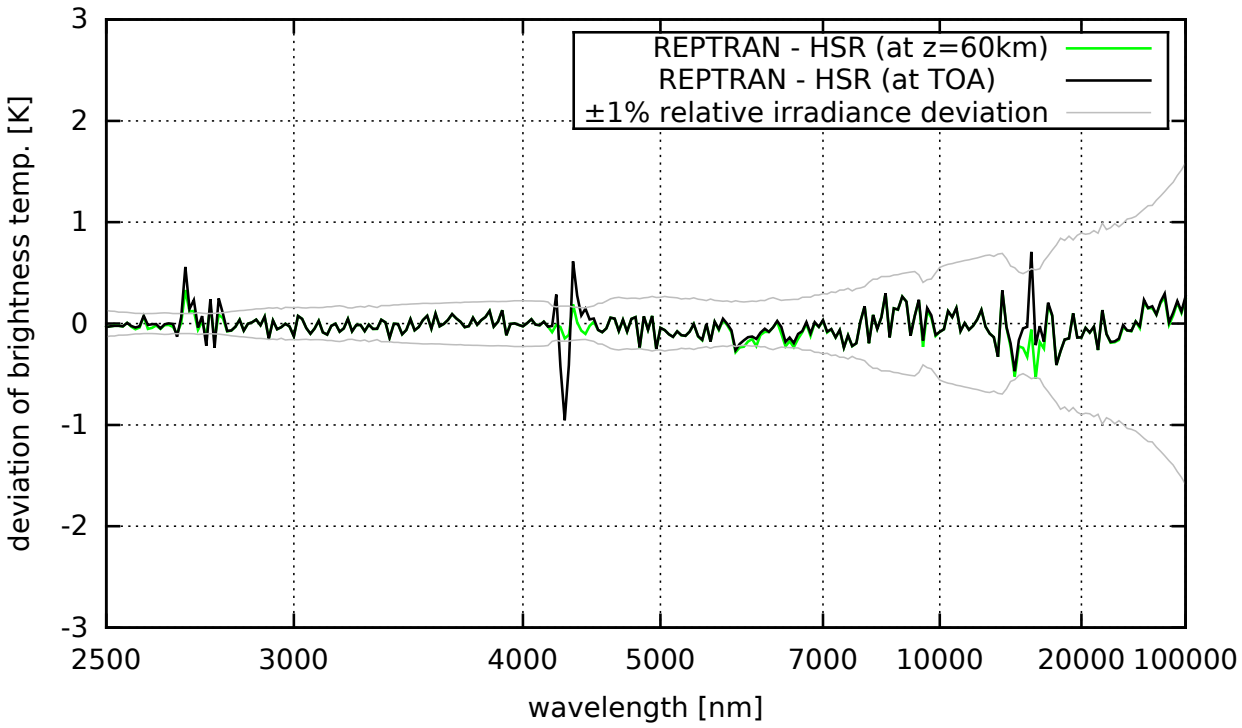

Figure 9: Deviations of brightness temperatures of upward irradiances at top of US standard atmosphere between REPTRAN parameterization and high spectral resolution calculations (HSR); the black line considers the complete profile up to z = 120 km, whereas the green line considers only heights up to z = 60 km; the surface albedo is set to 0.

Table 7: Root mean squared deviations (maximum) between the methods for brightness temperatures of upward irradiances in the thermal spectral range at top of different atmospheres; the surface albedo is set to 0.0.

atmosphere	REPTRAN - HSR	LOWTRAN - HSR
US standard	0.17 K (0.95 K)	2.86 K (10.6 K)
subarctic winter	0.17 K (0.80 K)	1.70 K (6.0 K)
subarctic summer	0.17 K (0.97 K)	2.55 K (9.0 K)
midlatitude winter	0.16 K (0.75 K)	2.19 K (7.9 K)
midlatitude summer	0.16 K (0.95 K)	2.80 K (9.4 K)
tropical	0.15 K (0.82 K)	2.99 K (9.6 K)
6 ECMWF atmospheres	0.21 K (1.60 K)	1.99 K (9.2 K)

Table 8: Root mean squared (maximum) deviations between the methods for direct solar irradiance at the surface for different atmospheres; the unit is mW m^{-2} $band^{-1}$.

atmosphere	REPTRAN - HSR	LOWTRAN - HSR
US standard	3.21 (20.3)	26.7 (199)
subarctic winter	2.57 (13.4)	23.2 (204)
subarctic summer	2.89 (18.8)	28.5 (198)
midlatitude winter	2.90 (20.7)	25.0 (202)
midlatitude summer	2.93 (17.1)	30.5 (208)
tropical	2.77 (17.6)	32.8 (231)
6 ECMWF atmospheres	2.93 (32.1)	22.8 (204)

After the inspection of two sources for deviations we now focus on the actual deviations of REPTRAN thermal bands from exact HSR results. The deviation of REPTRAN from HSR for the complete US standard atmosphere is typically on the order of 0.1 K, with maximum values close to 1.0 K (see black line in Fig. 9). The larger deviations occur mainly for bands where the described "top height effect" is relevant.

Tab. 7 shows mean and maximum deviations of REPTRAN from HSR for different atmospheric states. The deviations for most atmospheres are comparable with the deviations found for the US standard atmosphere, whereby slightly enhanced deviations are found for the ECMWF atmospheres. As mentioned above, the ECMWF atmospheres are characterized by a strong variability of temperature profiles. The deviations of LOWTRAN from HSR, also shown in Tab. 7, are approximately one order of magnitude larger than the deviations of REPTRAN from HSR.

3.5. Parameterized bands applied for surface irradiances

After investigating irradicances at the top of atmosphere, we now apply coarse bands parameterized with REPTRAN for simulating irradiances at the surface. We perform comparisons to exact HSR calculations analogous to the comparisons performed for the top of atmosphere. The application of REPTRAN at the surface potentially could result in large errors because the parameterized bands have been optimized for top of atmosphere radiances and might not capture spectral absorption features relevant at lower atmospheric levels. This issue will be investigated in the following.

3.5.1. Solar bands

Tab. 8 summarizes deviations of the parameterized band-integrated direct solar irradiances at the surface. The root mean squared deviations together with the maximum deviations are given for the coarse resolution bands. The mean deviation of REPTRAN from HSR does not vary significantly between the atmospheres and is close to 3 mW m^{-2} $band^{-1}$ with maximum values of 32.1 mW m^{-2} $band^{-1}$ for an ECMWF atmosphere. The mean relative deviation of REPTRAN from HSR is approximately 0.45% of the mean solar irradiance at the surface ($\approx$ 650 mW m^{-2} $band^{-1}$). At top of atmosphere, the mean relative deviation of the upward irradiance ($\approx$ 0.6 mW m^{-2} $band^{-1}$, Tab. 6) is approximately 0.3% of the mean upward irradiance ($\approx$ 200 mW m^{-2} $band^{-1}$). This indicates that the relative error for

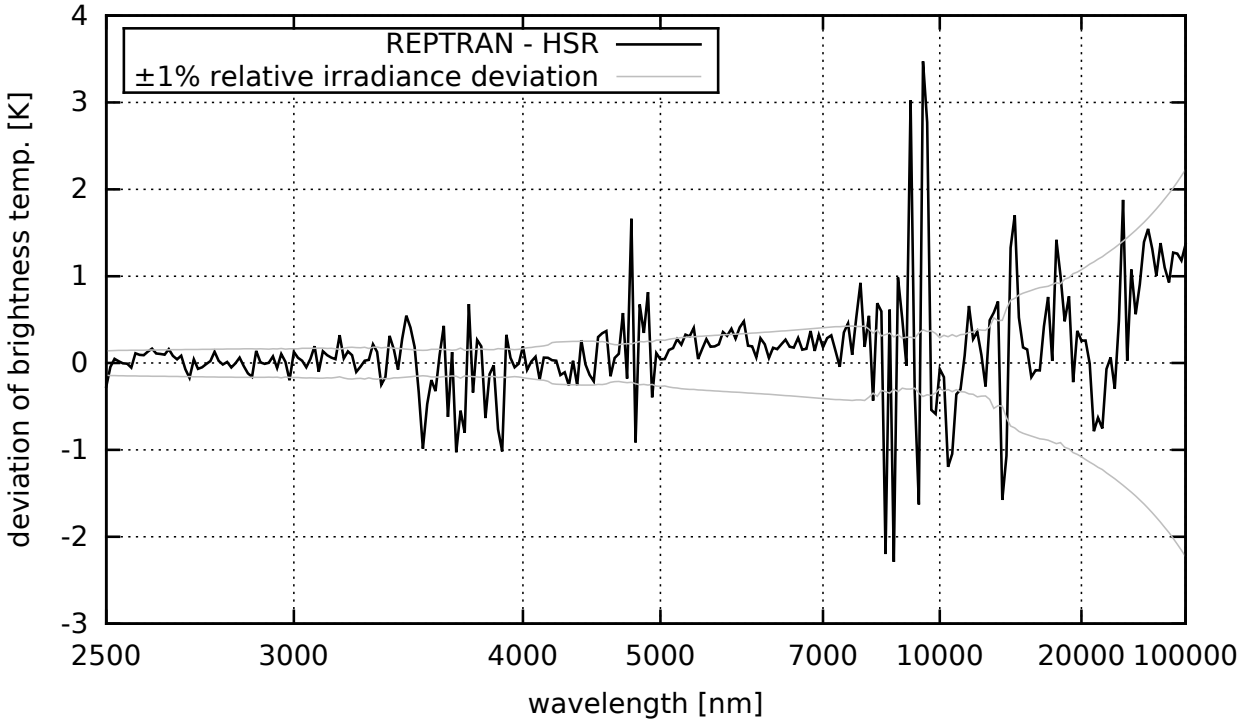

Figure 10: Deviations of brightness temperatures of downward irradiances at the surface of the US standard atmosphere; surface albedo is set to 0.0.

irradiances calculated using REPTRAN is only slightly larger at the surface than at the top of atmosphere. The good performance for solar irradiance at the surface is probably a result of the fact that most of the upward irradiance at top of atmosphere has been reflected by the surface and thus, like the irradiance at the surface, contains the spectral information from all atmospheric layers. The deviations of LOWTRAN from HSR are approximately one order of magnitude larger than the deviations found for REPTRAN, confirming that the REPTRAN parameterization performs comparatively well for solar irradiance at the surface, though it was not optimized for this setup.

3.5.2. Thermal bands

As the next step, we consider brightness temperatures of thermal downward irradiances reaching the surface. Fig. 10 shows deviations of brightness temperatures calculated using REPTRAN coarse thermal bands for the US standard atmosphere from exact HSR calculations. The deviations are largest at wavelengths where the brightness temperature is low. The deviation of REPTRAN from HSR reaches maximum values close to 3.5 K around λ = 10 μm. Comparison of the black line with the gray lines (1% lines) indicates that the maximum relative deviation of REPTRAN from HSR is on the order of 10%. There are some systematic deviations at wavelengths with strong absorption, mainly between 5 μm and 7.5 μm and wavelengths larger 40 μm. These deviations might be related to the difference of the spectral slopes of the radiances from blackbodies either having the temperature of the surface or the temperature of the uppermost atmospheric layers and the fact that the representative wavelengths for bands with strong absorption were selected to consider the spectral slope of the latter. Nonetheless, the relative deviation of the thermal irradiance at the surface is below 1% for a large fraction of bands.

Tab. 9 shows the root mean squared and maximum deviations of the brightness temperatures at the surface for different atmospheres. The deviations of all standard atmospheres are comparable with the deviations found for the US standard atmosphere. The deviations are slightly larger for the ECMWF atmospheres than for the standard atmospheres. A comparison of the brightness temperature deviations at the top of atmosphere (Tab. 7) and the surface (Tab. 9) reveals that the mean deviations of REPTRAN from HSR are approximately three times larger at the sur-

Table 9: Root mean squared (maximum) deviations between the methods for brightness temperatures of downward irradiances at the surface for different atmospheres; surface albedo is set to 0.0.

atmosphere	REPTRAN - HSR	LOWTRAN - HSR
US standard	0.61 K (3.47 K)	3.83 K (13.8 K)
subarctic winter	0.58 K (2.96 K)	3.97 K (12.3 K)
subarctic summer	0.53 K (3.11 K)	3.29 K (11.5 K)
midlatitude winter	0.60 K (2.64 K)	3.73 K (13.0 K)
midlatitude summer	0.56 K (3.55 K)	3.29 K (11.7 K)
tropical	0.57 K (3.51 K)	3.23 K (11.7 K)
6 ECMWF atmospheres	0.73 K (4.46 K)	4.29 K (14.9 K)

face than at the top of atmosphere. The mean deviations of LOWTRAN from HSR are typically 6-7 times larger than the deviations of REPTRAN from the HSR, showing a comparatively good accuracy of REPTRAN for thermal calculations also at the surface.

3.6. Parameterized bands applied for heating rates

Fig. 11 compares heating rate profiles calculated using the different approaches. It shows spectrally-integrated heating rates for thermal radiation in the wavelength range from 2.5 to 100 μm. The agreement between the approaches is reasonably good below 20 km with maximum deviations in the range of 0.2 K per day. The REPTRAN and LOWTRAN parameterizations however deviate significantly from HSR at high altitudes, in particular at heights $z > 40$ km. The main reason for the deviations at high altitudes is that the gas absorption spectrum contains very narrow and strong absorption lines at these altitudes which are captured by HSR calculations but not by the parameterizations. These very narrow and strong absorption lines are hardly relevant for spectrally-integrated radiances but have large effect on spectrally-integrated heating rates. Thus, for the representative wavelengths parameterization approach it seems plausible to assume that wavelengths with such strong absorption lines are hardly selected as representative wavelengths since the presented approach optimizes for radiances. Fig. 11 illustrates that neither REPTRAN nor LOWTRAN should be used for calculating heating rates at high altitudes. Using REPTRAN fine resolution bands instead of coarse bands does not significantly reduce the deviations of REPTRAN from HSR. Respective results for spectrally-integrated heating rates in the solar spectral range (not shown here) revealed a comparable height dependence of the deviations, that is only small deviations at lower altitudes and large deviations at high altitudes.

4. Conclusions

We adopted and optimized the representative wavelengths approach of Buehler et al. [11] for parameterizing spectral bands of different widths (1 cm^{-1}, 5 cm^{-1}, and 15 cm^{-1}), as well as for parameterizing spectral response functions of a large number of satellite channels. Solar as well as thermal radiation up to $\lambda = 100$ μm was considered. The parameterization approach considers gas absorption lines from the HITRAN spectroscopic data set in addition to continuum absorption from the MT_CKD model. It optimizes for spectrally-integrated radiances at the top of atmosphere with an accuracy threshold of 1% for a large set of highly variable states of the Earth's atmosphere. We implemented the parameterized bands and satellite channels as a new parameterization option (named "REPTRAN") in the freely available uvspec model and compared results from this implementation with results from high spectral resolution (HSR) calculations. We also compared results from the already-implemented LOWTRAN parameterization with HSR calculations.

From the application of REPTRAN it was found that:

1. Only few representative wavelengths are required to parameterize spectral integrals. Typically less than 10, and on average about 3 representative wavelengths are sufficient to fulfill the radiance accuracy threshold of 1%. The number of required wavelengths is largest (up to 22) in case of solar radiation and wavelengths larger than 2 μm (Fig. 3).
2. The uncertainty of REPTRAN for modeling of satellite channel responses is low (Tabs. 4, 5).

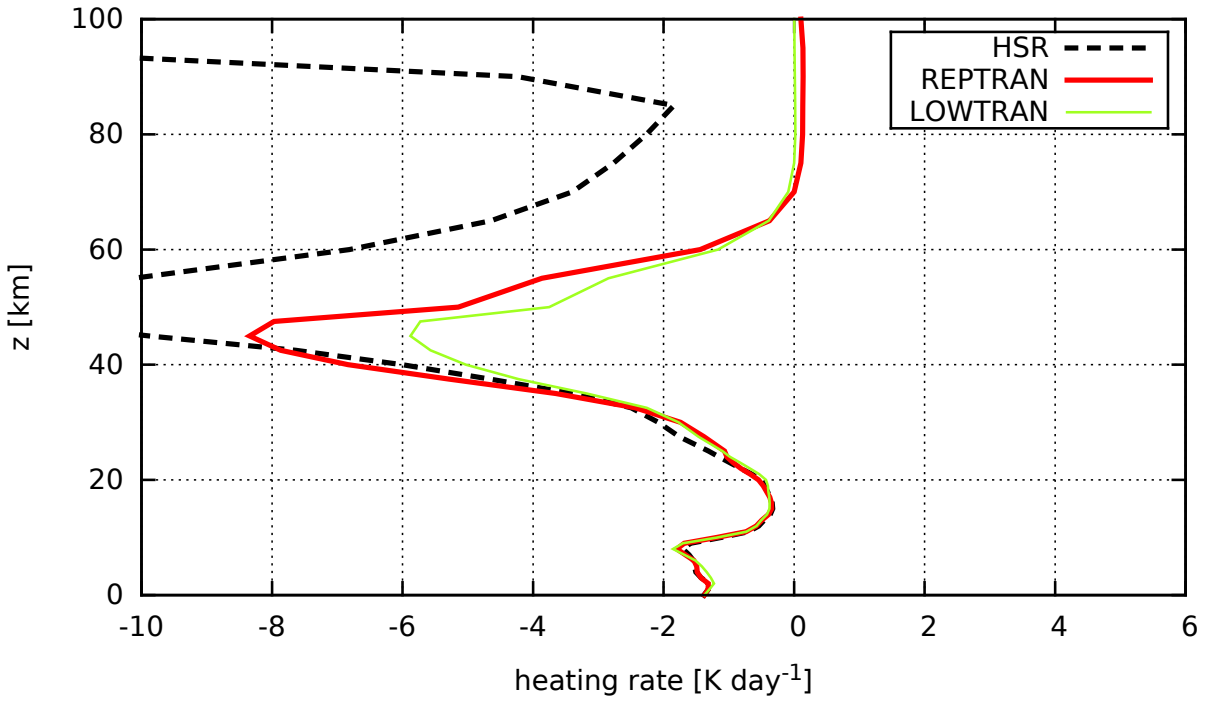

Figure 11: Heating rates in the US standard atmosphere due to thermal radiation in the spectral range from 2.5 μm and 100 μm using different modeling approaches; coarse resolution bands were used in case of REPTRAN; surface albedo is set to 0.0.

3. The comparisons for spectral bands revealed that the uncertainty of REPTRAN is low for both solar and thermal upward irradiance at the top of atmosphere as well as for solar irradiance at the surface (Tabs. 6, 7, 8).
4. The uncertainty of REPTRAN for thermal downward irradiance at the surface is higher than for thermal irradiance at the top of atmosphere, on average by a factor of 3. Nevertheless, the uncertainty of REPTRAN for thermal irradiance at the surface is still significanty lower than the uncertainty of the already-implemented parameterization (Tab. 9).
5. The uncertainty of thermal heating rates is comparable for REPTRAN and LOWTRAN. While the maximum deviations are in the range of 0.2 K per day in the troposphere and the lower stratosphere, significantly larger deviations from HSR calculations are found for both parameterizations at altitudes above 20 km (Fig. 11). The large deviations of REPTRAN can be understood as a result of its optimization for spectrally-integrated radiances and the fact that absorption lines at high altitudes are comparatively narrow and strong, affecting the spectrally-integrated heating rates much stronger than spectrally-integrated radiances.

When adding a new constituent to the atmospheric setup, the results from the application of the presented REPTRAN data might become unpredictable if the constituent exhibits a strong spectral variability that was not considered when parameterizing the spectral intervals. In most other cases, however, the presented REPTRAN parameterization approach provides quite low uncertainty for radiative transfer modeling of the Earth's atmosphere. Furthermore, it reduces significantly the computation time requirements compared with other approaches, in particular when modeling radiances of satellite radiometers. The REPTRAN parameterization data files for bands as well as satellite channels are provided at the libRadtran webpage - http://libradtran.org.

Acknowledgements

This study was funded by ESTEC under Contract AO/1-6607/10/NL/LvH (ESASLight II project). Spectral response functions of satellite instrument channels were provided by ESA.

Appendix A. List of parameterized satellite channel response functions

A list of parameterized satellite channels for solar radiation is given in Tab. A.10; channels parameterized for thermal radiation are given in Tab. A.11.

Appendix B. List of representative wavelengths for MSG3 channels

A list of representative wavelengths and weights for the channels of the MSG3 SEVIRI instrument is given for solar radiation source in Tab. B.12 and for thermal radiation source in Tab. B.13. They can be applied together with the absorption data described above. Representative wavelengths, their weights, and supplementary data can be extracted from the data available from the libRadtran webpage for any parameterized channel and band.

Table A.10: Satellite channel response functions parameterized for solar radiation.

satellite	instrument	channel name
ADEOS1	POLDER	443np 443p1 443p2 443p2 490np 565np 670p1 670p2 670p3 763np 765np 865p1 865p2 865p3 910np
ADEOS2	POLDER	443 443p 490 565 670p 763 765 865p 910
ALOS	AVNIR2	b1 b2 b3 b4
EarthCARE	MSI	b1 b2 b3 b4
Envisat	AATSR	ir37 v16 v555 v659 v870
Envisat	MERIS	ch01 … ch15
ERS1	ATSR	ir36 v16
ERS2	ATSR	ir36 v16 v555 v659 v870
Landsat1 … Landsat5	MSS	b1 b2 b3 b4
Landsat4 Landsat5	TM	b1 b2 b3 b4 b5 b7
Landsat7	ETM	b1 b2 b3 b4 b5 b7 b8
MSG1 MSG2 MSG3	SEVIRI	ch006 ch008 ch016 ch039
PARASOL	POLDER	1020 443 490 565 670 763 765 865 910
PROBA	CHRIS	a01 … a61, c01 … c18, h01 … h37 l01 … l18, l01a … l18a, w01 … w18
Sentinel3	OLCI	b02 … b21
Sentinel3	SLSTR	b1 … b7
Seosat		b1 b2 b3 b4
SPOT1 SPOT2 SPOT3	HRV	b1 b2 b3 pan
SPOT4	HRVIR	b1 b2 b3 b4 mono
SPOT4	VEGETATION1	b0 b2 b3 b4
SPOT5	HRG	b1 b2 b3 b4 pan
SPOT5	VEGETATION2	b0 b2 b3 b4

Table A.11: Satellite channel response functions parameterized for thermal radiation.

satellite	instrument	channel name
EarthCare	MSI	b7 b8 b9
Envisat	AATSR	ir11 ir12 ir37
ERS1 ERS2	ATSR	ir11 ir12 ir37
Landsat4 Landsat5	TM	b6
Landsat7	ETM	b6
MSG1 MSG2 MSG3	SEVIRI	ch039 ch062 ch073 ch087 ch097 ch108 ch120 ch134
Sentinel3	SLSTR	b7 b8 b9

Table B.12: Representative wavelengths $\lambda_{i_{\mathrm{rep}}}$ and weights $w_{i_{\mathrm{rep}}}$ optimized for different satellite channels and solar radiation source.

channel	i_{rep}	$\lambda_{i_{\mathrm{rep}}}$ [nm]	$w_{i_{\mathrm{rep}}}$	solar flux [mW m^{-2} nm^{-1}]
msg3_seviri_ch006	1	619.5815	0.586	1655
	2	664.4795	0.414	1567
msg3_seviri_ch008	1	796.2853	0.208	1129
	2	806.4738	0.792	1089
msg3_seviri_ch016	1	1584.574	0.134	225.3
	2	1639.934	0.459	228.8
	3	1652.107	0.228	229.9
	4	1684.948	0.179	212.9
msg3_seviri_ch039	1	3607.132	0.013	12.99
	2	3621.609	0.046	12.82
	3	3660.757	0.037	12.30
	4	3683.176	0.034	11.94
	5	3692.384	0.018	11.85
	6	3787.928	0.143	10.77
	7	3794.640	0.066	10.72
	8	3806.782	0.028	10.58
	9	3879.779	0.105	9.84
	10	3995.603	0.226	7.60
	11	4111.002	0.283	6.98

Table B.13: Representative wavelengths $\lambda_{i_{\mathrm{rep}}}$ and weights $w_{i_{\mathrm{rep}}}$ optimized for different satellite channels and thermal radiation source.

channel	i_{rep}	$\lambda_{i_{\mathrm{rep}}}$ [nm]	$w_{i_{\mathrm{rep}}}$
msg3_seviri_ch039	1	3690.930	0.099
	2	3704.772	0.295
	3	3874.026	0.137
	4	3942.741	0.019
	5	4005.412	0.265
	6	4152.224	0.139
	7	4214.193	0.036
	8	4237.213	0.009
msg3_seviri_ch062	1	6088.564	0.463
	2	6106.765	0.070
	3	6536.340	0.467
msg3_seviri_ch073	1	7228.371	0.450
	2	7376.566	0.061
	3	7481.678	0.262
	4	7508.143	0.123
	5	7559.400	0.104
msg3_seviri_ch087	1	8574.521	0.277
	2	8581.394	0.082
	3	8772.607	0.621
	4	8835.432	0.020
msg3_seviri_ch097	1	9550.629	0.277
	2	9661.430	0.431
	3	9716.618	0.247
	4	9785.438	0.044
msg3_seviri_ch108	1	10245.674	0.096
	2	10831.648	0.904
msg3_seviri_ch120	1	11872.122	0.837
	2	12285.149	0.163
msg3_seviri_ch134	1	12839.421	0.385
	2	13766.827	0.395
	3	13782.017	0.220

References

[1] A. A. Lacis, V. Oinas, A description of the correlated k distribution method for modeling nongray gaseous absorption, thermal emission, and multiple scattering in vertically inhomogeneous atmospheres, J. Geophys. Res. 96 (1991) 9027–9063. doi:10.1029/90JD01945.

[2] S. Kato, T. Ackerman, J. Mather, E. Clothiaux, The k-distribution method and correlated-k approximation for a shortwave radiative transfer model, J. Quant. Spectrosc. Radiat. Transfer 62 (1999) 109–121. doi:10.1016/S0022-4073(98)00075-2.

[3] Q. Fu, K. Liou, On the correlated k-distribution method for radiative transfer in nonhomogeneous atmospheres, J. Atmos. Sci. 49 (1992) 2139–2156. doi:10.1175/1520-0469(1992)049<2139:OTCDMF>2.0.CO;2.

[4] D. Kratz, The correlated k-distribution technique as applied to the AVHRR channels, J. Quant. Spectrosc. Radiat. Transfer 53 (1995) 501–517. doi:10.1016/0022-4073(95)00006-7.

[5] L. Doppler, R. Preusker, R. Bennartz, J. Fischer, k-bin and k-IR: k-distribution methods without correlation approximation for non-fixed instrument response function and extension to the thermal infrared - Applications to satellite remote sensing, J. Quant. Spectrosc. Radiat. Transfer 133 (2014) 382–395. doi:10.1016/j.jqsrt.2013.09.001.

[6] F. Kneizys, L. Abreu, G. Anderson, J. Chetwynd, E. Shettle, A. Berk, L. Bernstein, D. Robertson, P. Acharya, L. Rothman, J. Selby, W. Gallery, S. Clough, The MODTRAN 2/3 report and LOWTRAN 7 model, Tech. Rep. Contract F19628-91-C-0132, Phillips Laboratory, Air Force Base, Hanscom (1996).

[7] B. Mayer, A. Kylling, Technical Note: The libRadtran software package for radiative transfer calculations: Description and examples of use, Atmos. Chem. Phys. 5 (2005) 1855–1877. doi:10.5194/acp-5-1855-2005.

[8] L. S. Rothman, D. Jacquemart, A. Barbe, D. Chris Benner, M. Birk, L. R. Brown, M. R. Carleer, C. Chackerian Jr, K. Chance, L. H. Coudert, et al., The HITRAN 2004 molecular spectroscopic database, J. Quant. Spectrosc. Radiat. Transfer 96 (2005) 139–204. doi:10.1016/j.jqsrt.2004.10.008.

[9] S. Wacker, J. Gröbner, C. Emde, L. Vuilleumier, B. Mayer, E. Rozanov, Comparison of Measured and Modeled Nocturnal Clear Sky Longwave Downward Radiation at Payerne, Switzerland, in: T. Nakajima, M. Akemi Yamasoe (Eds.), American Institute of Physics Conference Series, 2009, pp. 589–592. doi:10.1063/1.3117055.

[10] A. Berk, G. P. Anderson, P. K. Acharya, L. S. Bernstein, L. Muratov, J. Lee, M. Fox, S. M. Adler-Golden, J. H. Chetwynd, M. L. Hoke, R. B. Lockwood, J. A. Gardner, T. W. Cooley, C. C. Borel, P. E. Lewis, MODTRAN 5: a reformulated atmospheric band model with auxiliary species and practical multiple scattering options: update, in: Proc. SPIE, Vol. 5806, 2005, pp. 662–667. doi:10.1117/12.606026.

[11] S. Buehler, V. John, A. Kottayil, M. Milz, P. Eriksson, Efficient radiative transfer simulations for a broadband infrared radiometer - combining a weighted mean of representative frequencies approach with frequency selection by simulated annealing, J. Quant. Spectrosc. Radiat. Transfer 111 (2010) 602 – 615. doi:10.1016/j.jqsrt.2009.10.018.

[12] L. Garand, D. S. Turner, M. Larocque, J. Bates, S. Boukabara, P. Brunel, F. Chevallier, G. Deblonde, R. Engelen, M. Hollingshead, D. Jackson, G. Jedlovec, J. Joiner, T. Kleespies, D. S. McKague, L. McMillin, J.-L. Moncet, J. R. Pardo, P. J. Rayer, E. Salathe, R. Saunders, N. A. Scott, P. van Delst, H. Woolf, Radiance and Jacobian intercomparison of radiative transfer models applied to HIRS and AMSU channels, J. Geophys. Res. 106 (2001) 24017 – 24031. doi:10.1029/2000JD000184.

[13] J. R. Key, P. Yang, B. A. Baum, S. L. Nasiri, Parameterization of shortwave ice cloud optical properties for various particle habits, J. Geophys. Res. 107 (2002) 4181. doi:10.1029/2001JD000742.

[14] P. Eriksson, S. Buehler, C. Davis, C. Emde, O. Lemke, ARTS, the atmospheric radiative transfer simulator, version 2, J. Quant. Spectrosc. Radiat. Transfer 112 (2011) 1551 – 1558. doi:10.1016/j.jqsrt.2011.03.001.

[15] S. Clough, M. Shephard, E. Mlawer, J. Delamere, M. Iacono, K. Cady-Pereira, S. Boukabara, P. Brown, Atmospheric radiative transfer modeling: a summary of the AER codes, J. Quant. Spectrosc. Radiat. Transfer 91 (2005) 233 – 244. doi:10.1016/j.jqsrt.2004.05.058.

[16] R. Buras, T. Dowling, C. Emde, New secondary-scattering correction in disort with increased efficiency for forward scattering, J. Quant. Spectrosc. Radiat. Transfer 112 (2011) 2028–2034. doi:10.1016/j.jqsrt.2011.03.019.

[17] R. Kurucz, Synthetic infrared spectra, in: Proceedings of the 154th Symposium of the International Astronomical Union (IAU); Tucson, Arizona, March 2-6, 1992, Kluwer, Acad., Norwell, MA, 1992.

[18] L. Molina, M. Molina, Absolute Absorption Cross Sections of Ozone in the 185- to 350-nm Wavelength Region, J. Geophys. Res. 91 (1986) 14501–14508. doi:10.1029/JD091iD13p14501.

[19] G. D. Greenblatt, J. J. Orlando, J. B. Burkholder, A. R. Ravishankara, Absorption measurements of oxygen between 330 and 1140 nm, J. Geophys. Res. 95 (1990) 18577–18582. doi:10.1029/JD095iD11p18577.

[20] J. P. Burrows, A. Dehn, B. Deters, S. Himmelmann, A. Richter, S. Voigt, J. Orphal, Atmospheric remote–sensing reference data from GOME: Part 1. Temperature–dependent absorption cross sections of NO_2 in the 231–794 nm range, J. Quant. Spectrosc. Radiat. Transfer 60 (1998) 1025–1031. doi:10.1016/S0022-4073(97)00197-0.

[21] S. Buehler, P. Eriksson, O. Lemke, Absorption lookup tables in the radiative transfer model ARTS, J. Quant. Spectrosc. Radiat. Transfer 112 (2011) 1559 – 1567. doi:10.1016/j.jqsrt.2011.03.008.

[22] G. Anderson, S. Clough, F. Kneizys, J. Chetwynd, E. Shettle, AFGL Atmospheric Constituent Profiles (0-120 km), Tech. Rep. AFGL-TR-86-0110, AFGL (OPI), Hanscom AFB, MA 01736 (1986).

[23] A. Kylling, K. Stamnes, S.-C. Tsay, A reliable and efficient two–stream algorithm for spherical radiative transfer: documentation of accuracy in realistic layered media , J. of Atmospheric Chemistry 21 (1995) 115–150. doi:10.1007/BF00696577.

[24] F. Chevallier, S. Di Michele, A. P. McNally, Diverse profile datasets from the ECMWF 91-level short-range forecasts, Tech. Rep. NWPSAF-EC-TR-010, European Centre for Medium-Range Weather Forecasts (2006).